DEVELOPMENT OF FLEXIBLE PROCEDURES FOR CO-OPTIMIZING DESIGN AND CONTROL OF FUEL CELL HYBRID VEHICLES

Marco Sorrentino[1], Valentina Cirillo, Liberato Nappi

Department of Industrial Engineering - University of Salerno, Via Giovanni Paolo II 132, 84084 Fisciano (SA) – Italy

ABSTRACT[2]

Developing successful fuel cell hybrid vehicles (FCHVs), to be destined to the widest deployment within the entire transport sector, is nowadays considered as a highly strategic target to fully meet well known environmental and regulatory constraints at international level. This happens thanks to the intrinsic overall superior features of fuel cell propulsion when compared to both electric and hybrid vehicles, such as high fuel-economy, reduced tank-to-wheel environmental impact and good ranges. Successful achievement of the above-introduced challenging goal motivates the research activity presented and discussed in this paper, namely the development of an advanced mathematical tool featuring co-optimization capabilities. The reason for such a requirement lies in the well-known strong interactions and mutual influence between selected design criteria and adopted control strategies. Therefore, a comprehensive model of a generic FCHV architecture and a specification independent control strategy, thus adaptable to different fuel cell system and battery sizes, were preliminary developed. Then, they were integrated and embedded within a modular constrained optimization algorithm, which was conceived in such a way as to simultaneously find the optimal FCHV powertrain design, as well as real-time applicable control strategies. Suitable design and energy management criteria were investigated on a selected driving cycle, in such a way to explore several powertrain configurations (i.e. more hybrid, as well as more plugin and range-extender like FCHV). This allowed verifying the suitability of the proposed procedure to yield solutions ensuring low hydrogen consumption (i.e. fuel economy as high as 135 km/kg) and full alignment with targeted energy management policies. Discussion of results, together with the physical meaning of main design and control variables provided as outcomes, underline the effectiveness of the

[1] Corresponding author's contacts: phone +39089964100; fax +39089964037; email msorrentino@unisa.it.

[2] https://doi.org/10.1016/j.enconman.2019.02.009

proposed tool in providing a solid support in the preliminary design of cost-effective fuel cell powertrains destined to a variety of applications and driving habits.

Keywords: Fuel Cell, Hybrid Vehicles, Energy Management, Specification Independency, Control, Co-optimization.

1. INTRODUCTION

The progressive depletion of primary energy resources reserves, together with air pollution and global warming issues, lead nations to impose progressively stringent regulations on greenhouse gas emissions, particularly on CO_2 ones. Within this debate, the impact of conventional vehicles is a particularly hot topic as, in major industrial countries, pollution generated by transportation generally averages more than 15% of a nation's total emitted pollution [1]. For instance, in 2010, the transport sector was responsible for over 30% of the final energy consumption of the EU27. Consequently, transport sector is widely recognised to be the major contributor to climate change, natural resource depletion and land fragmentation [2]. In fact, the direct combustion of fuel due to conventional transportation accounts for over half of greenhouse gas emissions and a significant fraction of air pollutant emissions [3], thus suggesting the development of alternative engineering solutions towards sustainable development. Hence, reducing the environmental impact of transport can be achieved by introducing new and cleaner technologies and shifting towards less environmentally damaging transport modes [1]. Particularly, the concepts of electrification and hybridization of cars are nowadays recognized as those to be pursued as soon as possible, because they represent the most viable way to reach the clean and sustainable development in transportation sector. In fact, according to different studies, hybridization has the potential to reduce the fuel consumption of gasoline ICE vehicles by 20-30% on standard U.S. drive cycles [4]. Hence, the sustainable transportation paradigm has become an increasingly popular solution, thanks to the favorable characteristics of high efficiency and low (or zero) emissions [5,6]. For instance, light duties vehicles impact for about 16% only [7] on global CO_2 emissions. Therefore, a transition from internal combustion engines vehicles towards electric and hybrid ones is a vital step in reducing humanities carbon footprint, especially in those countries where yet a large percentage of CO_2 is emitted from conventional vehicles [8,9]. When comparing all existing XEV powertrains, hydrogen fueled vehicles (either FCEVs or FCHVs) have more advantages over thermal hybrid vehicles (i.e. hybrid electric vehicles-HEVs), such as high fuel-economy (km/kg), related to the use of fuel with higher energy density, high efficiency and reduced environmental impact from a tank-to-wheel point of view. On the other hand, purely electric technology (i.e. electric vehicles-EVs) presents inferior autonomy and performance with respect to FCHV cars, due to the current technological limits of batteries, and may determine troublesome issues on electrical grid infrastructure [10]. Specifically, FCHVs have similar architecture of series hybrid vehicles [11], but they are equipped with a fuel cell system (FCS) and an electric motor that provides mechanical energy to the wheels. Structurally two blocks can be easily identified in the vehicle architecture: the former includes the on-board hydrogen storage system (i.e. battery technology), which is one of the most critical components since it influences vehicle acceleration and pure-electric driving range; the latter includes the technological devices, whose task is the generation of mechanical energy and its transmission to the vehicle itself. In fact, an electric motor uses electric energy generated by the chemical reactions taking place inside the fuel cells, which are arranged in series to form the stack. This reaction combines the hydrogen contained in the tank inside the car with the oxygen present in the air. The most common type of fuel cell for vehicle applications is the polymer electrolyte membrane (PEM) fuel cell, which benefits of several advantages, such as environment friendly working, simple working mechanisms, faster response times and affordable maintenance [12]. On the other side, lithium-ion batteries are the most reliable option for hybrid and electric vehicles. This battery typology is among the most performing systems, since it includes a wider field of applicability and operation than the other types of storage systems (e.g. high energy and high power). High power technologies are the preferred solution for FCHVs, but costs and risks need always to be considered when choosing the proper battery to install in the vehicle structure [13]. Despite the fact that FCS and batteries are often considered competitive technologies, FC systems can indeed fruitfully complement batteries. In fact, the electrification of vehicles allows FCs to be used as range extenders to overcome the key barrier to EV commercialization and range anxiety. Particularly, FCs offer various improvements to pure electric vehicles, such as range extension to more than 300 miles on a single fill, lower system weight, extended battery lifetime [14] and reduced re-charge times (i.e. shorter refilling periods). In addition, hydrogen vehicles have a tailpipe, but the only thing that comes out is water vapor. Hence, the chemical processes behind FCS allow propulsion without noxious emissions and, if the energy carrier is produced from renewable sources instead of fossil fuels (e.g. steam methane reforming from natural gas), the conversion of energy is essentially cleaner. Nevertheless, FCHV technology has not yet had significant market development, mainly due to the currently very expensive hydrogen production, as well as the absence of distribution and refueling infrastructures that will ensure the dissemination and distribution in a large scale. To tackle the above constraints, governmental and research institutions are now increasing the cooperation with main OEMs, as demonstrated by the growing awareness of EU funding bodies towards the high potential offered by FCHV-based hybridization, even in a short-term prospective [15]. Moreover, recent proposals of major automakers (Toyota [16] and Honda [17] show that hydrogen technology is overall ready to start a minimal competition to alternative sustainable mobility [18]. In fact, fuel cell vehicles appear as serious candidates for the substitution of gasoline cars, due to their capability of supporting the accomplishment of Kyoto Protocol and, besides, solving the oil dependence [19]. It is therefore important to focus on increasing the competitiveness of such vehicles in terms of fuel economy, thus overcoming the transitional problems related to hydrogen. In this context, the development of mathematical tools, which can potentially integrate in one single process the optimization of powertrain design and subsequent definition of real-time effective and applicable control strategies, can definitely contribute to speeding-up technological growth of XEVs [20], and particularly of FCHVs [15]. Moreover, the definition of development procedures, which are versatile enough to be deployed on FCHV powertrains with different degree of hybridization, are nowadays considered as a key factor to promote market penetration of hydrogen fueled cars, always taking into account various aspects concerning both the FC systems and the batteries technology (e.g. costs, reliability and durability [21]). Bizon [22] previously contributed on the development of online applicable optimization strategies, which are suitable to account for the impact of different and unpredicted road-load and driving conditions. Hu et al. [23] in their study stressed the importance of accounting for both battery size and real-time applicable control strategy definition, when aiming at achieving comprehensive optimization of FCHV functioning from both fuel saving and system durability point of view. Nevertheless, it is very important, in order to ensure fully considering the mutual interactions between components sizing and optimal management of hybrid vehicles, to co-optimize powertrain design and energy management, as addressed by Zhao and Sciarretta and Guo et al. in [24] and [25], respectively.

Following the above considerations on available state of the art, in the current work a mathematical tool is thus developed and applied to simultaneously accomplish optimal powertrain design and the definition of effective and reliable on-board applicable control strategies for light duty FCHVs. To authors knowledge, this is the first contribution aiming at co-optimized design and control of fuel-cell powered automotive systems. In the tool, a specification independent rule-based control strategy [26] is embedded, with the final aim of extending its applicability to a variety of powertrains and configurations [27], by means of suitable normalization/denormalization techniques. Indeed, such versatile and multi-purpose tools, based on extensive use of normalized models [28] and maps, can provide substantial contributions toward a greener transportation paradigm in many research fields [29].

The article is thus organized as follows: first, the basic equations, here utilized to assess mass impact of vehicle hybridization, as well as related traction power demand and hydrogen consumption, are briefly recalled. Afterwards, the specification independent control strategy is described, followed by the introduction of needed normalization and denormalization techniques to extend control strategies validity to other powertrain configurations. Subsequently, the available modeling and control tools are suitably integrated within a comprehensive optimization task, proved to be effective in co-optimizing the design and energy management of a variety of FCHV configurations.

2. METHODOLOGY

A procedure for the sizing of a fuel cell hybrid vehicle has been developed, mainly aiming at pointing out and promoting an alternative solution to traditional vehicles able to reduce their environmental impact. Particularly, a mathematical tool implemented in Matlab/Simulink® environment is used to design FCHVs guaranteeing same acceleration performance of reference conventional passenger cars, as well as the definition of control strategies that are appropriate to adequately account for the interaction with installed nominal power of involved powertrain components.

Figure 1 shows the FCHV architecture under analysis. The arrangement is a series hybrid configuration: the vehicle is driven only by the electric motor, while FC system supplies power, through the electric node (EN), both for battery recharging and vehicle traction. Figure 1 also illustrates the direction of energy flows: the battery (B) discharges and supplies energy to the electric motor (EM), which transforms the input energy from the electrical node (EN) into mechanical energy useful for the wheels. Whenever turned on, the electric fuel cell generator recharges the battery and might also directly provide electrical power to the wheels to ensure traction. As for the braking phase, the bottom scheme of Figure 1 highlights how regenerative braking is fruitfully enabled through the motor-wheels transmission, so as to recharge the battery, eventually in conjunction with the FCS whenever allowed by the adopted control strategy.

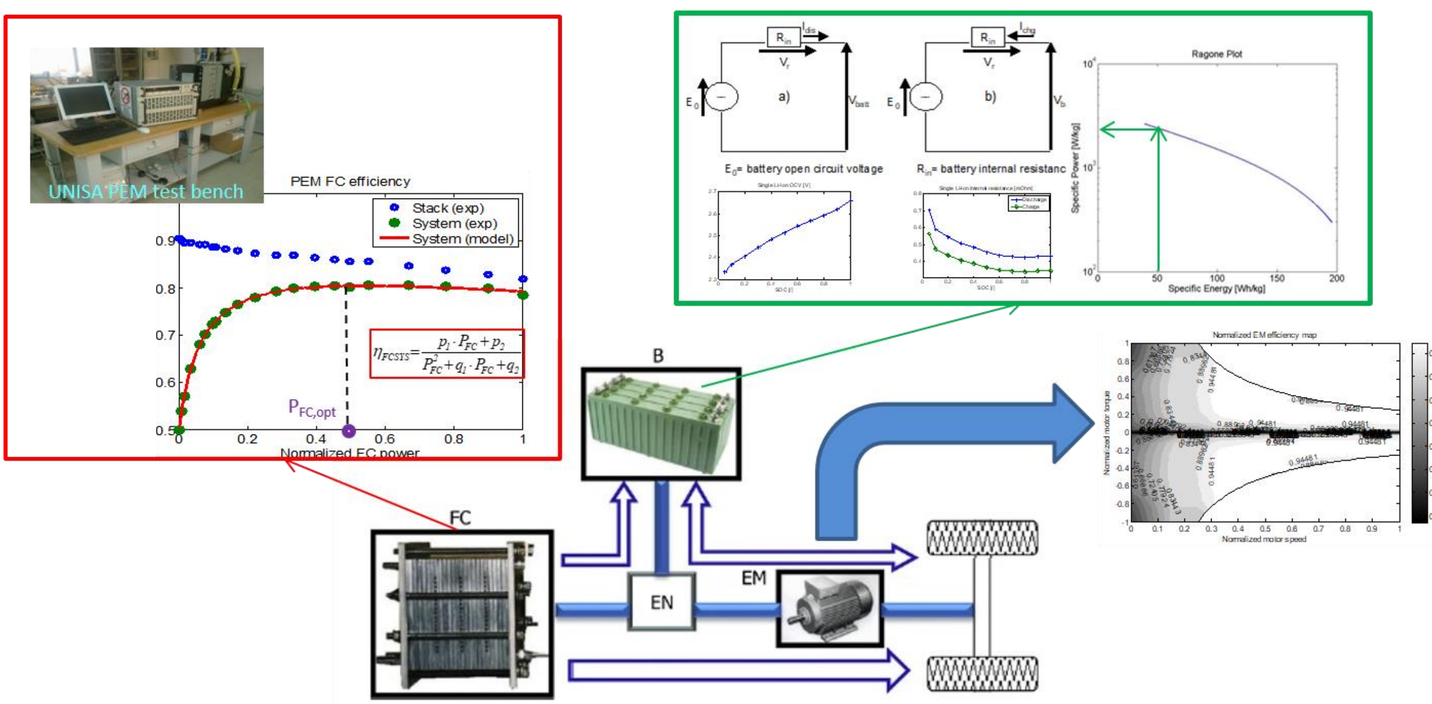

Figure 1: Fuel cell powertrain schematic (series architecture). Main experimental and literature-derived efficiency maps also are included and suitably associated to the specific powertrain component, for which they are used to model corresponding power flows and energy consumption in the FCHV comprehensive modeling structure (see section 2.1).

Figure 2 shows the mathematical tool structure for FCHV modeling. Particularly, it receives a large number of input variables, as described below:

• control variables, as provided by the proposed specifications independent control strategy for FCHV powertrains;

• design specifications, which consists in the hybrid fuel cell electric vehicle architecture and resulting power demand at wheels;

• exogenous variables, including unit masses and costs, feed-in-tariffs etc.;

All these fields interact with each other in order to achieve desired vehicle performance, while coping with energy savings and emissions reduction targets, by suitably determining installed FCS power and battery, specific energy. The last two design variables are selected through a suitable constrained optimization algorithm, which was conceived in such a way as to enable full exploration of most relevant FCHV powertrain architectures (i.e. full hybrid, plugin and/or range extender).

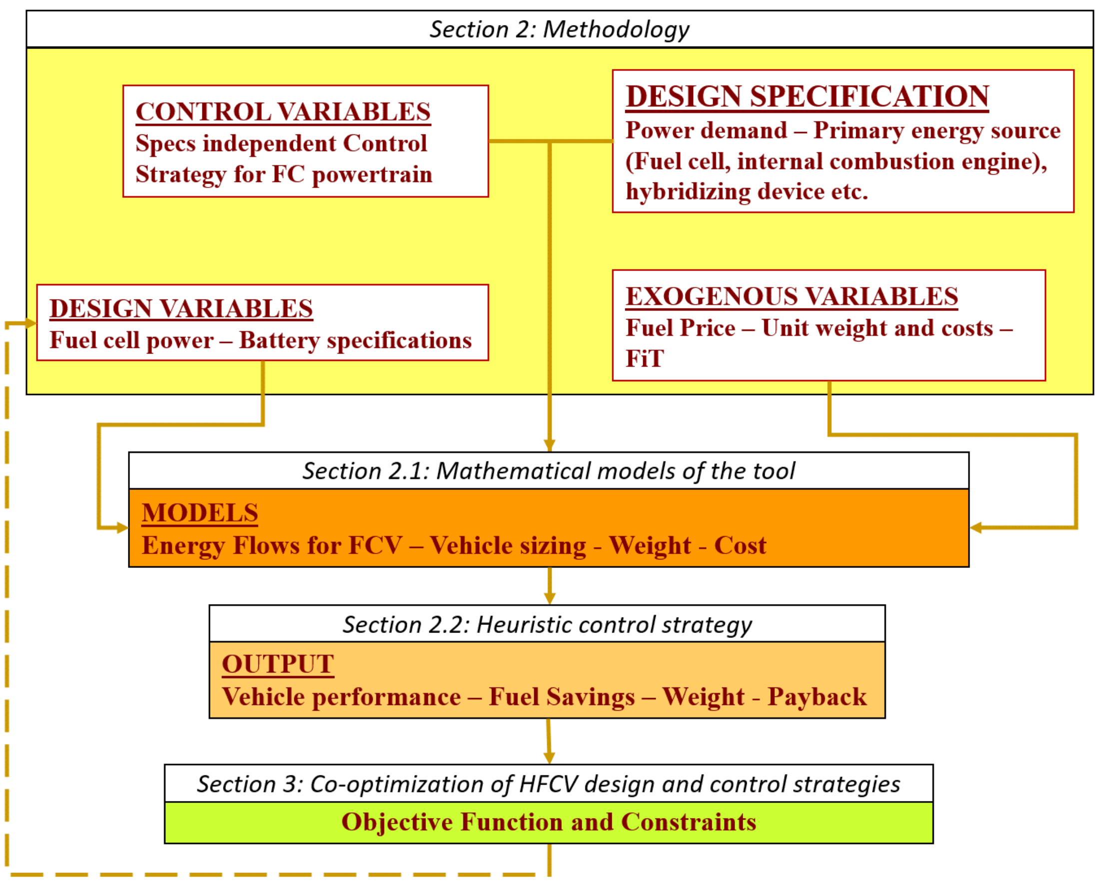

Figure 2: Structure of the mathematical tool here proposed and deployed to carry-out co-optimization analyses on FCHVs.

Specifically, the algorithm consists in a three-level cascade structure. Indeed, at the lower level performance parameters are calculated, including the *fuel economy* (FE), defined as the ratio between the traveled distance in the reference cycle and total fuel consumption (hydrogen in FCHV case):

$$FE = \frac{L}{\dot{m}_{H_2}}\left[\frac{km}{kg}\right] \tag{1}$$

This parameter has to be maximized in such a way as to determine optimal nominal FCS power and battery specific energy values. The mathematical tool is used to this end: the algorithm consists of a series of FCHV devices sub-models suitably integrated within a comprehensive hybrid vehicle simulator. Particularly, vehicle devices sub-models reproduce hybrid vehicle behavior subject to a given driving cycle. Indeed, a mass model determines the mass of the vehicle itself and a longitudinal dynamics model evaluates the power to be supplied to the wheels, instant by instant, in order to complete the assigned driving path. The outcomes yielded as for model configuration contribute to the definition of a control strategy placed at the higher level (Specification Independency, see section 2.2). Particularly, the proposed management strategy is a thermostatic control based on heuristic rules [11], whose reliability and effectiveness were suitably verified against dynamic programming and genetic algorithm offline reference benchmarks [26]: FC system switches on intermittently and recharges the battery in such a way as to meet the traction demand. Finally, at the top level, the optimization algorithm determines the value of the above-introduced design variables, thus contributing to the FCHV energy management and system design:

• FCS power (P^*_{FCS});

• Specific energy of the battery (E_{spec}).

These values are identified by solving a constrained minimization problem using a specific Matlab® resolution algorithm. The definition and resolution of this problem is the subject of section 3.

This section is divided into two sub-sections. The first proposes an overview of the mathematical tool under analysis by focusing on the design variables that the proposed algorithm investigates and by explaining how the FCHV devices modeling is accomplished. The latter describes the control strategy proposed for the FCHV energy management, conceived aiming at directly determining the heuristic rules, to be applied to suitably split the power demand between involved power sources, as a function of the optimal design variables.

2.1 Mathematical models

2.1.1 Mass model

A parametric model was used to assess the impact of hybridization on vehicle mass. Indeed, as detailed in the next sections, it is necessary to characterize vehicle mass and dimensions in order to finalize and implement its energy management strategy. The mathematical tool is based on a reference vehicle equipped with a thermal engine, defined as "conventional vehicle" (CV). Starting from the specifications of Table 1, a mass model is derived, aiming at evaluating the mass and other characteristics of the hydrogen vehicle by replacing conventional vehicle components by the devices required for its effective operation.

Table 1: Technical specifications of the reference conventional vehicle.

Lenght [m]	4.445
Width [m]	1.77
Height [m]	1.55
Wheel radius [cm]	28
Mass [kg]	1300
ICE power [kW]	75
M_T [kg]	8
Power to weight ratio (ρ_{PtW}) [kW/kg]	0.06

By referring to the vehicle architecture shown in Figure 1, the mass of a FCHV (M_{FCHV}) can be obtained by adding the mass of major hybridizing devices to the vehicle body mass (M_{body}). This latter is derived from the mass of the reference conventional vehicle (M_{CV}), by subtracting three contributions, due to the installed thermal engine, the original gear-box and the initial fuel tank, as follows:

$$M_{body} = M_{CV} - P^*_{ICE,CV} \cdot (m_{ICE} + m_{GB}) - M_T \quad (2)$$

Then, the vehicle mass can be determined by adding the hybridization devices that need to be installed on the hybrid vehicle, namely the fuel cell system, electric motor, battery pack and hydrogen tank:

$$M_{FCHV} = M_{body} + P^*_{FCS} \cdot m_{FC} + P^*_{EM} \cdot m_{EM} + M_{BC} \cdot N_{BC} + M_{HT} \quad (3)$$

Where P^* and m symbols correspond to nominal power and unit mass variables, respectively. Further details on value and meaning of each variable populating the right-hand side of Eq. (3) are retrievable from both paper nomenclature and Table 2. It is worth pointing out that hydrogen tank mass was estimated following the indications available in [30] and assuming a maximum driving range of 300 km, which conservatively corresponds to 3 kg of stored Hydrogen [17].

Table 2: Components unit specifications (i.e. masses and battery cell power) [10, 31].

m_{ICE} [kg·kW^{-1}]	2
m_{GB} [kg·kW^{-1}]	0.48
m_{EM} (mass of electric motor plus inverter) [kg·kW^{-1}]	1
m_{FCS} = [kg·kW^{-1}]	3.7
M_{HT} = [kg]	50
P_{BC} = single battery cell power [W·cell^{-1}]	1250

The number of battery cells (N_{BC}) is determined as follows (see Table 2):

$$N_C = \frac{P^*_{EM} - P^*_{FCS}}{P^*_{BC}} \tag{4}$$

It is finally worth remarking that a performance constraint shall be introduced, by imposing that the FCHV power to weight ratio (i.e. ρ_{PtW}) equals conventional vehicle one, thus ensuring FCHV guarantees the same CV acceleration performance:

$$\rho_{PtW} = \frac{P^*_{ICE}}{M_{CV}} = \frac{P^*_{EM}}{M_{FCHV}} \tag{5}$$

2.1.2 Longitudinal vehicle model

The adopted model investigates the dynamic behaviour of a vehicle that travels in a straight line by applying the second law of dynamics:

$$\begin{cases} F_m(t) = F_{res}(t) + M_e \cdot \dfrac{dv}{dt} \\ F_{res}(t) = F_g(t) + F_r(t) + F_a(t) \end{cases} \tag{6}$$

where $F_m(t)$ is the driving force, $F_{res}(t)$ is the resultant of the resisting forces that work against the motion and the last term of Eq. (6) represents the inertial action defined by the acceleration times the equivalent mass of the vehicle (M_e). Particularly, M_e equals $1.1 \cdot M_{HFCEV}$ to suitably account for rotational inertia [10]. During the acceleration phase, a driving force will be required, greater than the resistant one, while the reverse occurs in deceleration. Traction power is then estimated as follows, by multiplying each term of the first equation in (6) by the instantaneous speed:

$$P_{tr} = M_{FCHV} \cdot g \cdot v \cdot \left[C_r \cdot \cos(\alpha) + \sin(\alpha) \right] + 0.5 \cdot \rho \cdot C_x \cdot A_v \cdot v^3 + M_e \cdot \frac{dv}{dt} \cdot v \tag{7}$$

in which the different forces opposing the motion appear: weight force (F_g), rolling resistance (F_r), which is the frictional force opposing the rolling motion of the wheels, and aerodynamic resistance (F_a), which is the resistance opposed by air to the vehicle movement. Particularly, some of the variables depicted into Eq. (7) need to be clarified. M_{FCHV} represents the mass of the vehicle and, α is the slope angle of the road surface, v is the actual speed of the vehicle and A_v represents the frontal area calculated from the vehicle dimensions. Furthermore, g is the gravitational acceleration, C_r represents the coefficient of rolling friction of the tires, ρ is the air density and C_x is the drag coefficient, whose values are included in Table 3.

Table 3: Main variables used in the battery model for traction power estimation.

Cr [-]	0.01
Cx [-]	0.33
ρ [kg/m^3]	1.18

2.1.3 Battery model

The operation of a hybrid technology is closely linked to storage batteries. A compromise between costs, mass and capacity of the accumulators need to be found in the design of the vehicle itself. In fact, the choice of the right battery technology is fundamental in the sizing of hybrid electric vehicles. Particularly, one of the main issue is the need to increase the battery capacity and, at the same time, decrease the overall vehicle weight, in such a way as to optimize the vehicles performances and extend their range autonomy. Obviously, it is also important to consider the economic aspect, so as to guarantee a non-excessive cost of the energy storage system. Furthermore, batteries lifetime and ageing phenomena are relevant aspects, which should always be taken into account when designing the battery system and, therefore, implementing a battery model. In fact, batteries are usually subject to different abuse conditions during their usage in EVs (e.g. temperature variations, humidity, vibrations, driving operating conditions etc.). Specifically, several factors may affect negatively their life cycle. For instance, multiple charge and discharge cycles undergoing during batteries operation, as well as deep discharge phases, may shorten battery lifetime, thus causing a possible premature failure or reducing their performances and durability. Hence, an appropriate control device should be integrated in the vehicle structure in such a way as to monitor critical parameters and ensure safe battery operation. The following design variables are used in the mathematical tool:

• Specific energy [Wh/kg], which is calculated by comparing the energy that can be stored in the battery to its mass. Particularly, a high specific energy value allows to increase the energy that can be stored in a system, with the same mass, and consequently a greater autonomy is met;

• Specific power [W/kg], which is obtained by comparing the power that the accumulator is able to deliver to its mass. High discharge power ensures high driving performance.

Specific energy and specific power are linked to each other through a particular chart, called Ragone plot. It consists in a plan used for performance comparison of various energy-storing devices; in fact, on such a chart the values of specific energy [Wh/kg] are plotted versus specific power [W/kg]. Both axes are logarithmic, which allows comparing performance of very different devices (i.e. extremely high and extremely low power). Specifically, lithium ion batteries are the most performing ones because they include a wider field of applicability and operation than the other types of accumulators, as shown on the right side of the green rectangle in Figure 1. In fact, Li-Ion batteries are used in the mathematical model for the hybrid traction;

• Capacity [Wh], which represents the energy accumulated in the battery. Analytically it is the product of number of cells per capacity of the single cell;

• Capacity [Ah], which is the amount of charge that a battery can deliver at a rated voltage. Particularly, it is defined as the product of the current intensity supplied for the time needed to completely discharge the battery to a definite current value. Analytically it is calculated as the ratio between the capacity of the single cell [Wh/cell] and the discharge voltage [V], fixed at a defined value;

• State of charge (SOC), which is the percentage of residual energy stored in the batteries instant by instant, normalized with its total capacity [Ah]. Particularly, the mathematical tool can estimate its value following a specific physical model, which relies on Kirchhoff's laws. Indeed, the battery system may be represented by an ideal open-circuit voltage generator in series with an internal resistance R_{in}, as shown on the left side of the green rectangle in Figure 1. Since OCV and Li-Ion internal resistance mathematically depends on the state of charge, the algorithm evaluates battery voltage (V_{batt}) value by applying Kirchhoff's laws to the equivalent circuit as follows, once the initial SOC value is known:

$$V_{batt} = OCV - R_{in} I \tag{8}$$

Then, battery electric power is estimated by multiplying each term of (8) for the current variable, thus obtaining the following formula:

$$P_{batt} = V_{batt} \cdot I = OCV \cdot I - R_{in} \cdot I^2 \tag{9}$$

Once battery power and initial SOC values are known, the battery model in real time usage is able to estimate the current value by solving Eq. (9) and, consequently, the SOC on the basis of the real electric power, whose value is positive for discharge phase and negative for the charge one. Particularly, the reference equation for battery SOC evaluation is given above:

$$SOC = -\frac{1}{Q_{TOT}}\int I(t)dt + SOC(t_0) \tag{10}$$

where Q_{TOT} is the overall capacity of battery in Coulomb.

• Number of cells, which is calculated through the following balance equation at the electric node of the vehicle with nominal powers:

$$P_B + P_{FCS} = P_{EM} \tag{11}$$

$$N_C \cdot P_{BC} = P_B = P_{EM} - P_{FCS} \tag{12}$$

Where P_{EM} is the power demand to be met by the electric motor, P_{BC} is the nominal power of the battery single cell and P_B is the battery stack power. Therefore, the number of cells is reduced when P_{FC} increases, thus requiring a higher propulsion demand to the engine but also a lower capacity of the battery pack, that behaves as a buffer.

2.1.4 Electric motor model

The efficiency of the selected AC induction electric motor technology is computed by means of normalized maps derived from the model based library proposed in Rousseau [31]. Indeed, an energy balance at the electrical node allows evaluating, instant by instant, the electrical power arriving to the EM or departing from it and the respective mechanical power, supplied (motor behavior) or recovered (generator behavior for the battery). The analysis of the power balance at EN (see Eq. (11) in 2.1.3) clearly shows that the positive traction power shall be equal to the useful one of the electric motor; in fact, for non-negative P_{tr} values, the mechanical power to be supplied by the EM is (see Figure 1):

$$P_{EM} = \frac{P_{tr}}{\eta_{tr}} \qquad \text{if } P_{tr} \geq 0 \tag{13}$$

P_{EM} can also be expressed as a function of fuel cell system and battery power, as follows:

$$P_{EM} = \eta_{EM} \cdot \left(P_{FSC} + P_B\right) \qquad \text{if } P_{tr} \geq 0 \tag{14}$$

On the other hand, when P_{tr} is negative, the regenerative braking mode is active, resulting in the following expression for the electrical energy delivered by the EM:

$$P_{EM} = \eta_{tr} \cdot \eta_{EM} \cdot P_{tr} \qquad \text{if } P_{tr} < 0 \tag{15}$$

where the η variables correspond to efficiency terms. During regenerative braking, battery can be charged by the fuel cell system, thus the following equation holds for negative P_{tr} values:

$$P_B = P_{EM} - P_{FCS} \qquad \text{if } P_{tr} < 0 \tag{16}$$

2.1.5 PEM fuel cell system efficiency model

The general definition of FC system efficiency is the one resulting from the following formula, which considers the stack power and the one absorbed by auxiliaries, both function of the FC system power:

$$\eta_{FCS} = \frac{P_{stack} - P_{aux}}{\dot{m}_{H_2} \cdot HHV_{H_2}} = \frac{P^*_{FCS}}{\dot{m}_{H_2} \cdot HHV_{H_2}} \tag{17}$$

where $\dot{m}_{H_2}$ represents the hydrogen flow [kg/s] required for the FC operation and HHV_{H2} is the higher heating value of hydrogen, equal to 141.9 MJ/kg. The FCS was modeled using a specific efficiency map, developed and presented in (see red rectangle in Figure 1) [10].

2.2 Versatile specifications independent control strategy

This section describes the control strategy used for the energy management of a hybrid fuel cell vehicle; particularly, it allows selecting the control variables in order to guarantee proper, highly efficient and GHG friendly FCHV driving. Indeed, at the highest level of the optimization algorithm the control strategy acts, thus allowing creating maps according to variables normalization/denormalization rules by using model data and optimal vehicle design outcomes (i.e. design variables and vehicle-adapted energy management strategies).

2.2.1 Rules definition

Hybrid vehicle energy management is determined through a rule-based algorithm, defined as "specifications independent control strategy", which follows the two heuristic rules proposed in [26] and then extended to fuel cell vehicles in [10], relying on thermostat-based management of FCS. Particularly, the vehicle normally starts in electric mode and keeps being powered this way until the battery state of charge status reaches a minimum threshold SOC_{lo} (i.e. charge-depleting phase, as shown in Figure 3). When this latter value is reached, the FCS is turned-on to supply power for both propulsion and battery pack recharging. As soon as the state of charge reaches the upper limit SOC_{up}, the FCS is switched off and the vehicle gets back to electrical mode.

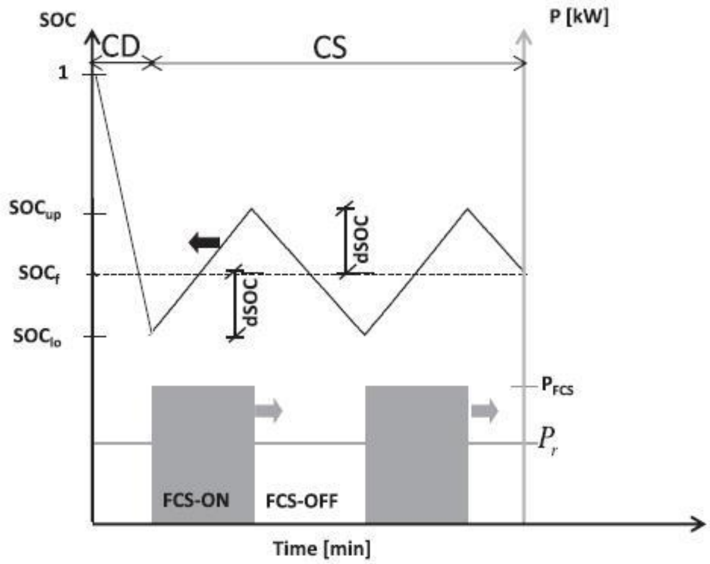

Figure 3: Qualitative description of typical thermostat-based management of FCS in FCHV powertrains.

During this phase, an oscillation of the state of charge (dSOC) occurs around a fixed SOC_f value, thus resulting in an overall charge sustaining management of the battery pack. Particularly, SOC_f is usually set to 0.7 [32] for the light duty vehicle range (LDV), so as to guarantee, together with a proper choice of the oscillation window dSOC, a safe and efficient us of the battery pack. The described procedure continues until the end of the driving cycle.

The control variables to be selected from the strategy are the two following ones: the instantaneous electric power provided by the FC system ($P_{FCS,supply}$) and the dSOC (maximum allowable oscillation around targeted battery state of charge-SOC). The optimal values of $P_{FCS,supply}$ and dSOC are estimated online as functions of the average traction power demand:

$$P_{FCS,\sup ply} = f\left(\overline{P}_{tr}\right) \tag{18}$$

$$dSOC = g\left(\overline{P}_{tr}\right) \tag{19}$$

The selection of the optimized parameters is carried-out by identifying the minimum hydrogen mass consumed over an assigned timeframe, obtained by concatenating two consecutive time-windows, during which FCS is active and inactive, respectively. Indeed, by solving the following minimization problem over an extended range of average traction-power demand, it is possible to find the optimal f and g functions:

$$\min_{P_{FCS,\sup ply},\Delta t_{FC-OFF}} \int \dot{m}_{H2}\left(P_{FCS,\sup ply},\Delta t_{FCS-OFF}\right)dt \tag{20}$$

Subject to the constraint:

$$SOC(end) = SOC_f \tag{21}$$

Solving the above minimization problem corresponds to identifying the best engine intermittency (i.e. $\Delta t_{FCS\text{-}OFF}$, which is the time interval, during which FCS is kept off) and the power level at which the fuel cell system should work for a given average traction power demand $\overline{P_{tr}}$. This latter variable is estimated, exploiting the increasing reliability of a-priori speed prediction-based methods [33], over an assigned timeframe [26], here set to t_h=10 min as shown in Figure 4.

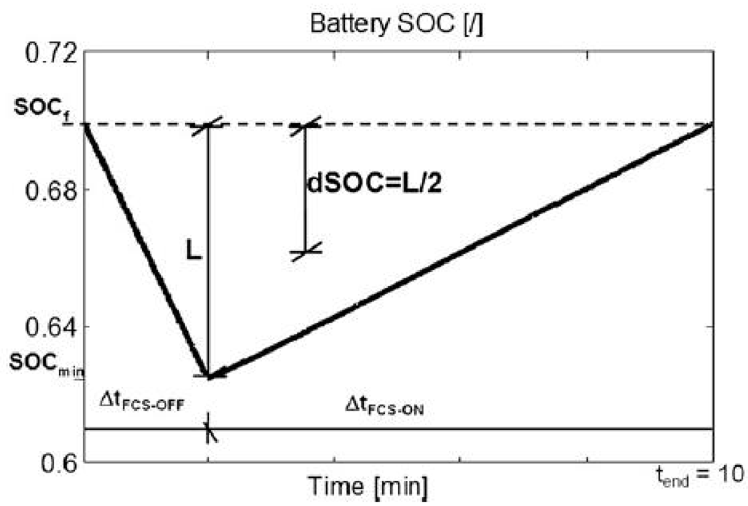

Figure 4: schematic representation of the proposed SOC indirect determination from the optimal SOC trajectory, for an assigned $\overline{P_{tr}}$ value (see Eqs. 19-20).

As a result of the optimization strategy, the battery state of charge is linear (see Figure 4). In fact, after a certain value of required traction power is set, the fuel cell system charges the battery by delivering a specific power for a certain period of time. Then, the charge sustaining procedure ensures a final SOC value not excessively reduced, thus avoiding an extreme discharge depth and, consequently, contributing not to compromise the useful life of the battery. The optimization algorithm yields on output two maps associated to Eqs. (18) and (19), as shown in Figure 5. They express the power that FCS shall supply and the dSOC drift to be realized before engine is turned off/on, depending on an average traction power required to the wheels. Particularly, in this study several maps pairs were obtained through the above described optimization, each corresponding to a different degree of hybridization (DH), defined as follows:

$$DH = \frac{P^*_{batt}}{P^*_{FCS} + P^*_{batt}} \tag{22}$$

Specifically, this variable corresponds to the ratio between rated battery and electric motor power, which is defined as the sum of both fuel cell system and battery contributions. In fact, both energy sources contribute to drive the electric motor of the series vehicle, as the powertrain schematic of the implemented vehicle model clearly shows in Figure 1. Indeed, different FCHV specifications are assumed to derive the optimized rules maps for varying nominal fuel cell system power, while keeping constant the power to weight ratio. Each optimized map is normalized, in such a way as to become potentially extendable to different degrees of hybridizationm, because variables standardization technique allows obtaining solutions that are congruent from the physical point of view for any choice of the variables to be optimized, even if they are of different orders of magnitude, as discussed later on. Specifically, y-axis normalization of the map relating to $P_{FCS,}$supply is obtained as the ratio of Eq. (18) data divided by nominal fuel cell system power (see Eq. 23), whereas Eq. (24) is here proposed to account for the impact of larger/smaller battery size when extending a map optimized on different FCS power values:

$$P_{FCS,\sup ply,norm} = \frac{P_{FCS,\sup ply}}{P^{*}_{FCS}} \tag{23}$$

$$dSOC_{norm} = dSOC[\%] \cdot Cap_{BATTref}[kWh] \tag{24}$$

It is worth noting that in Eq. (24) $Cap_{BATTref}$ represents the battery capacity [kWh] of the powertrain, on which the optimization was performed. Thus, Eq. (24) allows introducing specification independency in optimal thermostatic management of FCHV, provided that rule extension is accomplished by appropriately rescaling the dSOCnorm with respect to new powertrain specifications. The latter aspect, which actually corresponds to the denormalization phase, is described in detail in the following (see section 2.2.2).

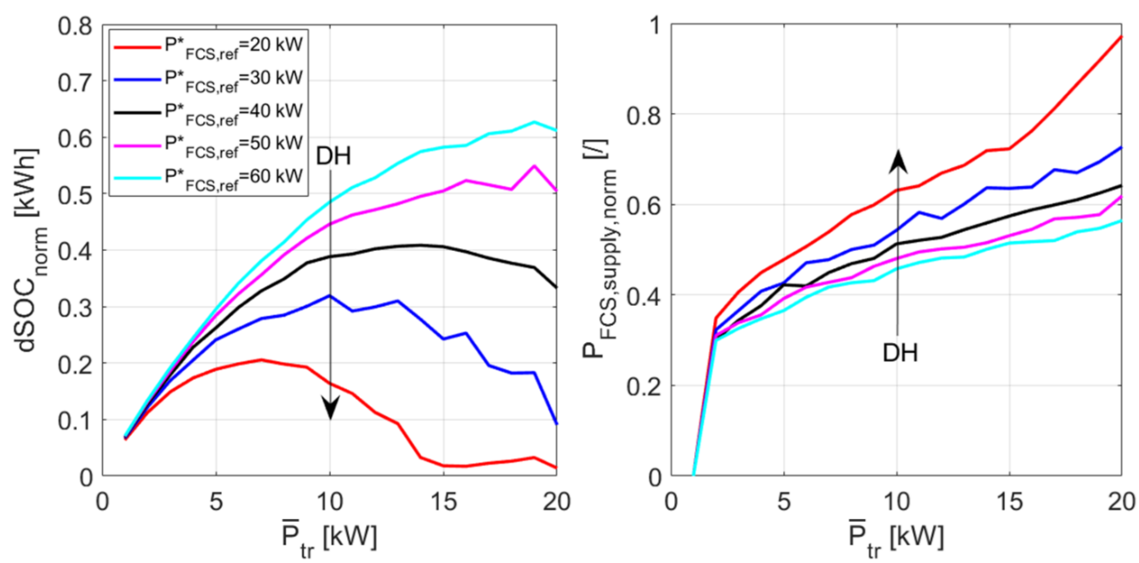

Figure 5: Normalized maps of FCHV powertrain control variables [34].

For all vehicles, normalized fuel cell power exhibits a monotonic increase. This behavior could in principle appear unexpected, as commonly fuel cell systems work at best efficiency at relatively low power. Nevertheless, the fact that fuel cell system efficiency falls quite close to its optimal value, in a wide range [35], justifies the above-noticed general load following behavior for fuel cell supply power map. Moreover, right-hand side plot in Figure

5 indicates that fuel cell power supply does not differ significantly at low traction power, whereas the discrepancy between one map and another becomes larger as $\overline{P_{tr}}$ increases. This is mostly due to the normalization effect (see Eq. 23). More interesting, from the physical point of view, is the dSOC$_{norm}$ map behavior, illustrated in the left side of Figure 5. Particularly, at low traction power the optimization algorithm proposes, independently from degree of hybridization, monotonically increasing behavior. This happens thanks to the sudden increase in fuel cell power supply in these conditions, as shown in the right-hand side graph, which particularly guarantees easily achieving charge sustaining behavior. Then, varying DH impact starts increasing beyond $\overline{P_{tr}}$=3 kW and continues up to significantly high $\overline{P_{tr}}$ values. In fact, vehicles with a low degree of hybridization can afford working with higher dSOC$_{norm}$ excursions, thanks to the higher power that can be supplied by the FC system. Then, after $\overline{P_{tr}}$=15 kW the increasing trend reduces and the dSOC$_{norm}$ sets on a plateau region. On the other hand, vehicles with higher degree of hybridization can afford an increasing dSOC$_{norm}$ trend within a smaller $\overline{P_{tr}}$ range, as well as with reduced slope (e.g. P^*_{FCS}=40 kW). After reaching a maximum, for such powertrains it is necessary to reduce dSOC$_{norm}$ excursions to meet charge-sustaining constraint (see Eq.18). The values of dSOC$_{norm}$ for P^*_{FCS} =20 kW, however, are very close to zero when $\overline{P_{tr}}$ values are high (e.g. over 10 kW). This behavior leads to a physical non-sense because the power given by the fuel cell system becomes lower than that required. As a result, the dSOC$_{norm}$ slope is significantly reduced. In fact, urban/suburban driving are mostly characterized by $\overline{P_{tr}}$ lower than 10 kW on average.

2.2.2 Maps normalization and denormalization

Once vehicle specifications are determined, extension of one of the optimal rules maps, presented and discussed in the previous section, firstly entails normalizing the x-axis, which represents traction power demand. X-axis normalization is accomplished according to Eq. (25), by dividing average traction power demand the reference FC power (P^*_{FCref}), which assumes values between 20 and 60 kW as discussed above:

$$P_{tr,norm} = \frac{\overline{P}_{tr}}{P^*_{FCSref}} \tag{25}$$

Then, the respective denormalization can be obtained by simply multiplying the right hand side of Eq. (25) by the P^*_{FCS} of the vehicle, which the map is extended to:

$$P_{tr,denorm} = \frac{\overline{P}_{tr}}{P^*_{FCSref}} \cdot P^*_{FCS} \tag{26}$$

As for maps ordinates (see Figure 5), such values are denormalized by referring to the normalization definitions given above (see Eqs. 23 and 24):

$$P_{FCS,\sup ply} = P_{FCS,\sup ply,norm} \cdot P^*_{FCS} \tag{27}$$

$$dSOC_{denorm} = \frac{dSOC[\%] \cdot Cap_{BATTref}[kWh]}{Cap_{BATT}[kWh]} \tag{28}$$

3. CO-OPTIMIZATION OF FCHV DESIGN AND CONTROL STRATEGIES

This section describes the mathematical procedure, through which the scenario analysis of the powertrain and the FCHV design were conducted. Specifically, the optimization algorithm ensures that a series of solutions, which are parameterized for each value of the maximum recharge time of the battery (t_{max}), are attained by applying the appropriate initial conditions on the variables to be optimized. Indeed, a specific scenario can be defined for each t_{max} value, thus analyzing the FCHV behavior through the identification of a specific control strategy for each solution, as described below (see section 4). Particularly, once the system under examination and all its components have been defined, the constrained optimization problem has to be numerically solved in order to establish the best possible energy mix and the design associated with the vehicle's propulsion sources. The numerical resolution allows searching the global maximum of a defined mathematical function and, consequently, the optimal values of the nominal FCS power, as well as the battery specific energy of the battery: an appropriate objective function, which depends on the design variables, is thus defined. In this specific case study, the objective function corresponds to the fuel economy:

$$\max_{P^*_{FCS},\, E_{spec}} FE = \max_{P^*_{FCS},\, E_{spec}} \frac{L}{m_{H_2}} \tag{29}$$

Optimization deals with selecting, overall, the best option among a number of possible choices that are feasible and do not violate constraints. In fact, this optimization problem, defined by Eq. (29), has an objective that the algorithm attempts to maximize: fuel consumption has to be minimized, by modifying the two design variables in accordance with specific constraints. Indeed, the variables values for the optimal solution are subject to an unilateral constraint condition on the battery charging time during post-driving (PD):

$$t_{PD,charge} \leq t_{\max} \tag{30}$$

where the maximum PD charging time of the battery (t_{max}) assumes the values of 100, 200 and 300 s in the analysis. Moreover, Eqs. (31) and (32) introduce both lower and upper bounds for the design variables, so that the optimal solution is found in accordance with the following ranges:

$$P_{FCS}^{*} \in [5,60] \qquad [\mathrm{kW}] \tag{31}$$

$$E_{spec} \in [40,180] \qquad \left[\frac{\mathrm{Wh}}{\mathrm{kg}}\right] \tag{32}$$

It is worth remarking that the inclusion of eq. (30) among all constraints is motivated by the interest towards exploring both pure- or mostly-hybrid configurations, i.e. capable of ensuring final state of charge as much close to the target SOC_f as possible, as well as plugin or even range extender like configurations. Such a choice, beyond being motivated by the increasing awareness worldwide of the need of providing auto-makers with the most versatile simulation tools, so as to reliably verify cost effectiveness of different FCHV solutions and configurations, also enables the assessment of the opportunities linked to range extender like sizing strategies [36]. Figure 6 shows a qualitative example of the described numerical procedure, obtained from the resolution of the optimization problem. Particularly, the battery SOC trend in time is illustrated. It is assumed that the vehicle under examination travels along a certain driving path with a fixed length (L) and the time required to complete the cycle is called t_{drive}. The path along which the optimization takes place is obtained from the union of 10 ECE15-EUDC cycles, 11700 s long. Each cycle consists of four urban cycles where the peak speed reaches 50 km/h and an extra-urban cycle with a maximum speed of 120 km/h. The optimization algorithm verifies the final value of the battery state of charge at the end of the driving cycle: if SOC_f value is lower than the reference one, equal to 0.7, it is possible to recharge the battery in post-driving phase. With this respect, is worth remarking that the objective function to minimize is calculated as the length of the driving path, expressed in km, divided by the hydrogen consumption, which is not evaluated simply as the fuel mass depleted during the cycle. In fact, the denominator variable of fuel economy is calculated as the sum of the hydrogen mass used to complete the reference driving path (m_{drive}) and the hydrogen consumption linked to battery recharge during post-driving (m_{charge}):

$$m_{H_2} = m_{drive} + m_{charge} \tag{33}$$

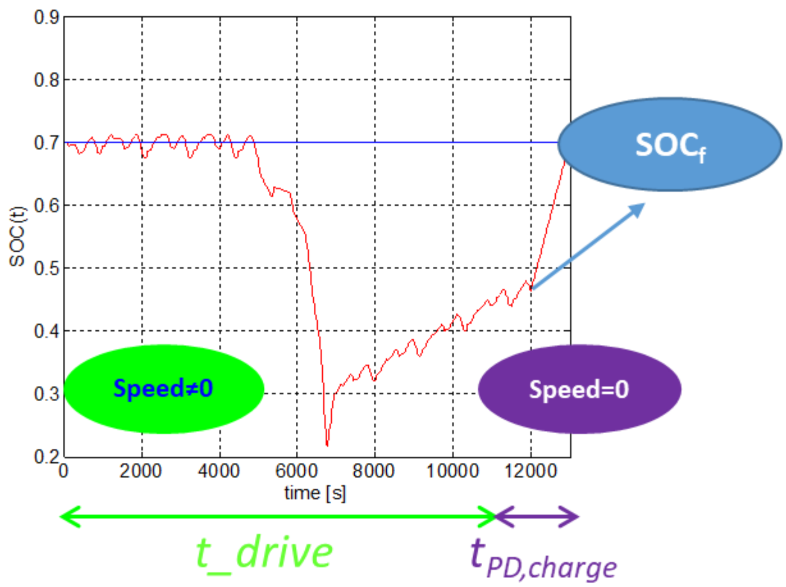

Figure 6: Physical meaning of the PD battery charging time.

Battery state of charge initially keeps close to the targeted value final (i.e. 0.7), then it drops considerably before the end of the driving cycle. Soon after vehicle stops, the battery is fully recharged at constant FCS power. Particularly, SOC value at the end of the cycle decreases as the maximum recharge time increases: if charging time is longer, battery does not need to be recharged excessively during the cycle, since the achievement of the reference SOC will be reached off-line when the vehicle has stopped after the driving cycle.

The effective charging time of the battery ($t_{PD,charge}$) is defined as the ratio between the energy needed to recharge the battery (E_{charge}) and corresponding power that the fuel cell system shall provide (P_{charge}) for this recharging process, as expressed in the following formula:

$$t_{PD,charge} = \frac{E_{charge}}{P_{FCS,charge}} \cdot 3600 \qquad [\mathrm{s}] \tag{34}$$

Where both E_{charge} and P_{charge} are calculated according to the optimal values of the two optimized variables (P_{FCS}^* and E_{spec}) obtained from the problem resolution. Specifically, E_{charge} is calculated as follows:

$$E_{charge} = \frac{(0.7 - SOC_f) \cdot Cap_{Batt}}{\overline{\eta}_{Batt}} \cdot 1000 \qquad [\mathrm{Wh}] \tag{35}$$

where SOC_f is the final state of charge value of the battery at the end of the cycle, Cap_{Batt} is battery capacity in kWh, $\bar{\eta}_{BATT}$ is battery average efficiency (here assumed equal to 0.97). On the other hand, Eq. (36) is here proposed to express the charging power definition:

$$P_{FCS,charge} = 0.45\ P_{FCS}^{*} \cdot 1000 \qquad [W] \tag{36}$$

Therefore, the power at which the battery is charged corresponds to a percentage of FCS power, which identifies its maximum efficiency operating condition (see Figure 1).

4. RESULTS AND APPLICATION-ORIENTED OUTCOMES

The powertrain design performed through the optimization algorithm determines the optimal values of the above introduced P_{FCS}^{*} and E_{spec} variables, by solving a two degrees of freedom constrained problem. The objective function to be maximized is the fuel economy, as described in section 3, and is subject to different initial conditions. Therefore, considering the constraint introduced via Eq. (30), a double parametric analysis is accomplished: the former examines the influence of initial conditions on design and performance variables, whereas the latter studies the change in the solutions resulting from relaxing the constraint on post-driving battery charging time (see Eq. 34). Moreover, the influence of versatile control rules selection was assessed. As shown in Figure 5, 5 pairs of normalized control maps are available. A previous study [34] indicated the maps developed assuming FCS nominal power of 20 and 30 kW as the most energy-effective ones. Therefore, the optimization task was repeated twice, one per each pair of normalized control maps embedded in the overall optimization framework sketched in Figure 7, as underlined in Table 4. Particularly, Figure 7 aims at providing a general overview of the proposed co-optimization algorithm. Starting from the assigned initial conditions, an iterative process based on the Matlab® fmicon tool is initiated towards convergence to the cost function minimum. In parallel, the versatile rule-based energy management strategy is continuously adapted to current design variables, in such a way as to directly embed, in the current driving cycle simulation, the control maps that are candidate to be optimal for the configuration under investigation. Afterwards, the resulting outcomes, both in terms of design (i.e. P_{FCS}^{*} and E_{spec}) and operating (i.e. $t_{PD,charge}$) variables are verified against assigned cost-function and constraints (see section 3). Upon successful assessment, the optimization task can be safely terminated; associated outcomes will thus be recorded as the solution of the set co-optimization task, aimed at determining vehicle best configuration and related real-time applicable control strategies.

Table 4: Main assumptions and input data considered in the two optimization tasks run in the presented research activity.

OPTIMIZATION TASK	$P^*_{FCS,ref}$ of normalized control maps	t_{max}	Initial conditions		Number of optimization analyses
			$P_{FCS}{*}_{,0}$	$E_{spec,0}$	
1	20 [kW]	100 [s] 200 [s] 300 [s]	8.5 9 9.5 10	65 85 105 125	48
2	30 [kW]				48

The outcomes of the Figure 7 accomplished optimization tasks, as yielded on output by the above-introduced co-optimization algorithm when applied to the new European driving cycle (NEDC), are synthesized and deeply analyzed in Figure 8 through Figure 11. It is worth remarking that a series of 10 NEDC driving mission was assumed, in such a way as to test a realistic case where hybrid vehicles are definitely more useful than pure electric ones, i.e. when requested distance range is high.

The comparison between the two adopted normalized maps, illustrated in Figure 8, highlights how the one developed with reference to a 20 kW FCS (see section) always outperforms the 30 kW one in terms of fuel economy (see Figure 8a). This happens either considering the best case or the value averaged on all the initial conditions pairs listed in the fourth column of Table 4. Such an outcome can be explained considering that a larger FCS tend towards a more full-power like fuel cell vehicle configuration, thus being capable of meeting the highest acceleration request mostly with the fuel cell system, as confirmed by Figure 11b. This will inevitably sacrifice the higher FCS efficiency guaranteed by plugin or range extender like configurations [36]. Another positive feature of the 20 kW-derived normalized map, also emerging from Figure 8, resides in the lower sensitivity of both best case and averaged solutions to the change in tmax, whereas the relaxation of $t_{PD,charge}$ constraint (see Eq.34) has a more evident impact when the 30kW-derived map is adopted. A further aspect, to be underlined when analyzing Figure 8c and Figure 8d, is linked to the extremely low values of battery capacity and Espec yielded on output in all analyzed scenarios. Such a result is strictly related to the specific high-power battery technology considered in this paper [31]. Sticking to the high-power region of the Ragone plot (see Figure 2) enables the optimization procedure to limit vehicle mass increase due to hybridization. This occurs while moving towards highly electrified (i.e. high degree of hybridization) solutions, as also confirmed by the ordinate values of Figure 10c. Figure 8b shows indeed that, despite the expected increase in P_{FCS}^* resulting from strengthening the $t_{PD,charge}$ constraint, yet the installed optimal P_{FCS}^* keeps relatively low. The latter comments are surely specific of assumed hypotheses on battery technology;

nevertheless, the discussed physical meaning of optimal solutions confirms the effectiveness and reliability of the proposed design procedure.

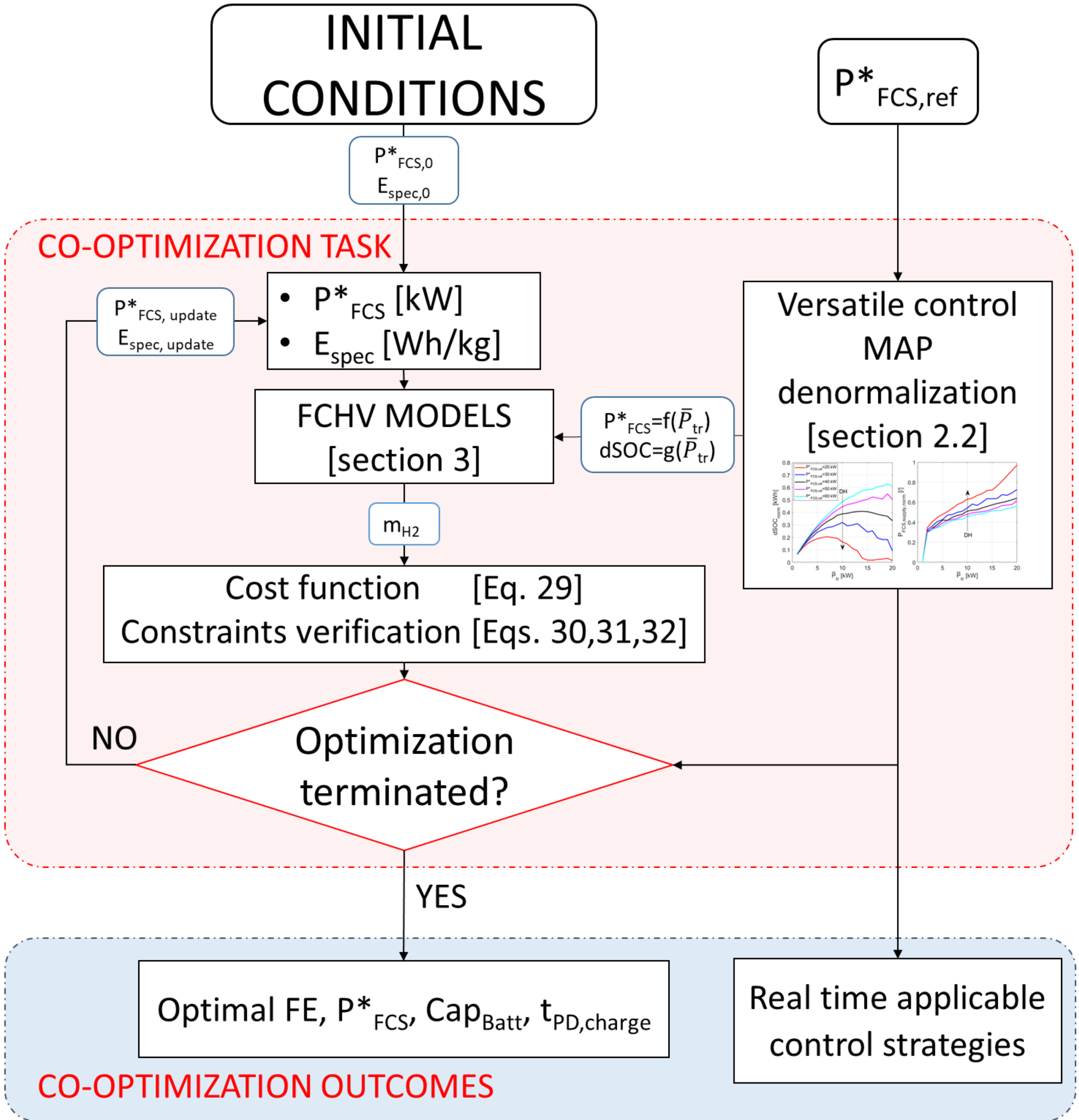

Figure 7: Flow-diagram illustrating the logic and main input to outcomes paths characterizing the proposed model-based co-optimization tool for real-world effective design of FCHV powertrains.

Focusing on Figure 8b and Figure 8c, two opposite trends characterize the variation of the two design variables as a function of assigned maximum $t_{PD,charge}$. To better appreciate the consequences of these trends in terms of design guidelines, Figure 9 shows all the configurations yielded by the co-optimization tool in case 1 of Table 4, thus allowing concentrating the analysis on the most effective normalized versatile control strategy. As expected, smaller t_{max} values cause P_{FCS}^* to increase significantly (i.e. to double in the specific case dealt with in this paper) and battery capacity to shrink appreciably, thus allowing fully meeting the post-driving charging constraint. Such a behavior actually consists in moving from a plug-in-like configuration towards a more hybrid one, as limiting or even eliminating the opportunity of completing battery re-charging in post-driving means that the battery itself has to be designed as an energy buffer.

Figure 10 shows the relationship between a key simulated variable, i.e. the final SOC achieved at the end of the driving phase (SOC_f), and both design (P_{FCS}^* and DH) and operating (i.e. effective $t_{PD,\ charge}$) variables. As expected, the more charge sustaining the strategy (i.e. the higher the SOC_f), the higher the installed FCS power (Figure 10a) and the lower the $t_{PD,charge}$ (Figure 10b) and DH (Figure 10c). Therefore, recalling the trend shown in Figure 9, the shift towards the lower P_{FCS}^* and the higher battery capacity, induced by the explored range of t_{max} values, suggests the designer to work on the progressive transition from a hybrid to a more electric configuration, with a consequent increase in the degree of hybridization.

Finally, Figure 11 shows the time trajectories of the main powertrain variables, namely battery SOC (Figure 11a) FCS power contribution (Figure 11b) and vehicle power demand (Figure 11c). As mentioned above, the powertrain configuration determined in case of stringent $t_{PD,charge}$ constraint is able to supply a larger contribution by the FCS, especially in correspondence of most significant vehicle accelerations (see Figure 11c). Such an aspect, together with the tendency of the control strategy to increase FCS contribution at the very end of the cycle (see Figure 11b), demonstrates the successfulness of combining a-priori estimation of vehicle power demand at the wheels with the proposed versatile rule-based energy management. Such a strategy indeed allows fully exploiting available installed power, especially in case of the more hybrid solution (i.e. the one obtained setting t_{max}=100 seconds), with the aim of reducing as much as possible the post driving charging phase duration and successfully meet all constraints introduced in section 3. As for the fuel economy, it is clear from Figure 11a and Figure 11b that the more plugin solutions (i.e. corresponding to t_{max}=200 s and 300 s) tend to let the FCS work for a longer time as compared to the more hybrid one. From Figure 11a, it particularly emerges that such an energy management strategy allows increasing the operating time in which the FCS work close to the maximum efficiency point, even at the end of the driving cycle, where the need of bringing the SOC as close as possible to the desired value (i.e. 0.7) is more relevant. On the other hand, in case of the more hybrid configuration the minimum FCS power (around 4 kW, one fourth of P_{FCS}^*) is farther from the maximum efficiency point as compared to the other best cases. This aspect, which explains the lower fuel economy of more hybrid powertrain configurations, should be assessed in conjunction with the fact that the P_{FCS}^{*} value is obtained only in case of more plugin configurations. The fact that the maximum power is never exploited by the more hybrid solution indicates that the optimal configuration satisfies the performance constraint introduced in the mass model (see Eq. 3), but it is not capable of finding the best trade-off with battery-related added mass limitation. Such a trade-off is instead perfectly met by the plugin-like configurations. This is a relevant finding, to be carefully accounted for by FCHV developers during preliminary design of such innovative powertrains. Another positive feature of the more plugin configurations emerges from Figure 11a: SOC derivative in charging mode is always smoother than the more hybrid solution, thus ensuring better battery energy management from the lifetime viewpoint. It is finally worth remarking that the optimization algorithm (see Figure 7) yields on output vehicle configurations of similar overall mass in the three analyzed best cases, as it emrges from the comparion of power demand trajectories in Figure 11c.

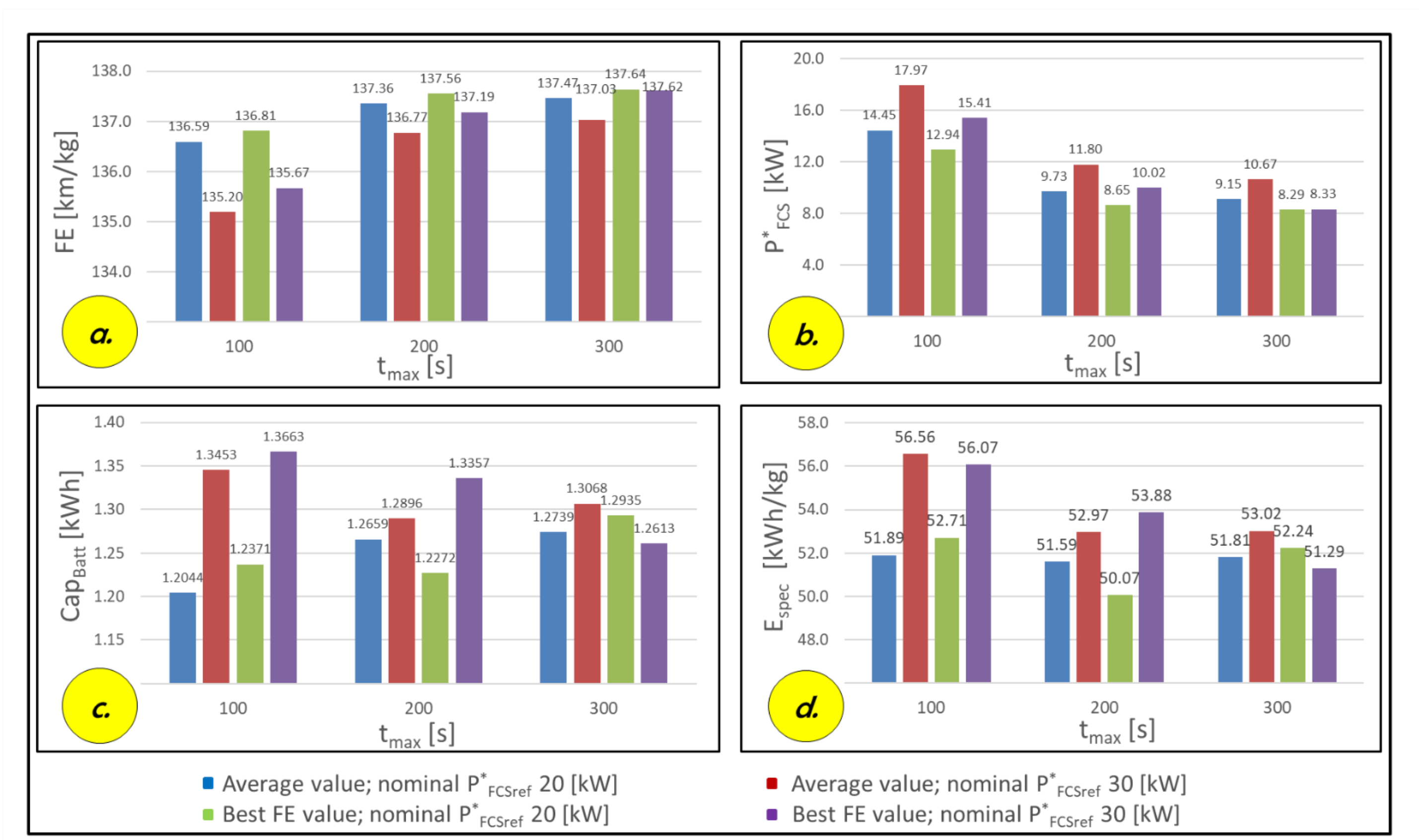

Figure 8: Average (over the entire set of initial conditions explored (see Table 4) and Best FE values of main optimized variables: a) Fuel economy [km/kg], b) Fuel cell system power [kW], c) Battery capacity [kWh], d) Battery specific energy [Wh/kg]. It is worth remarking that

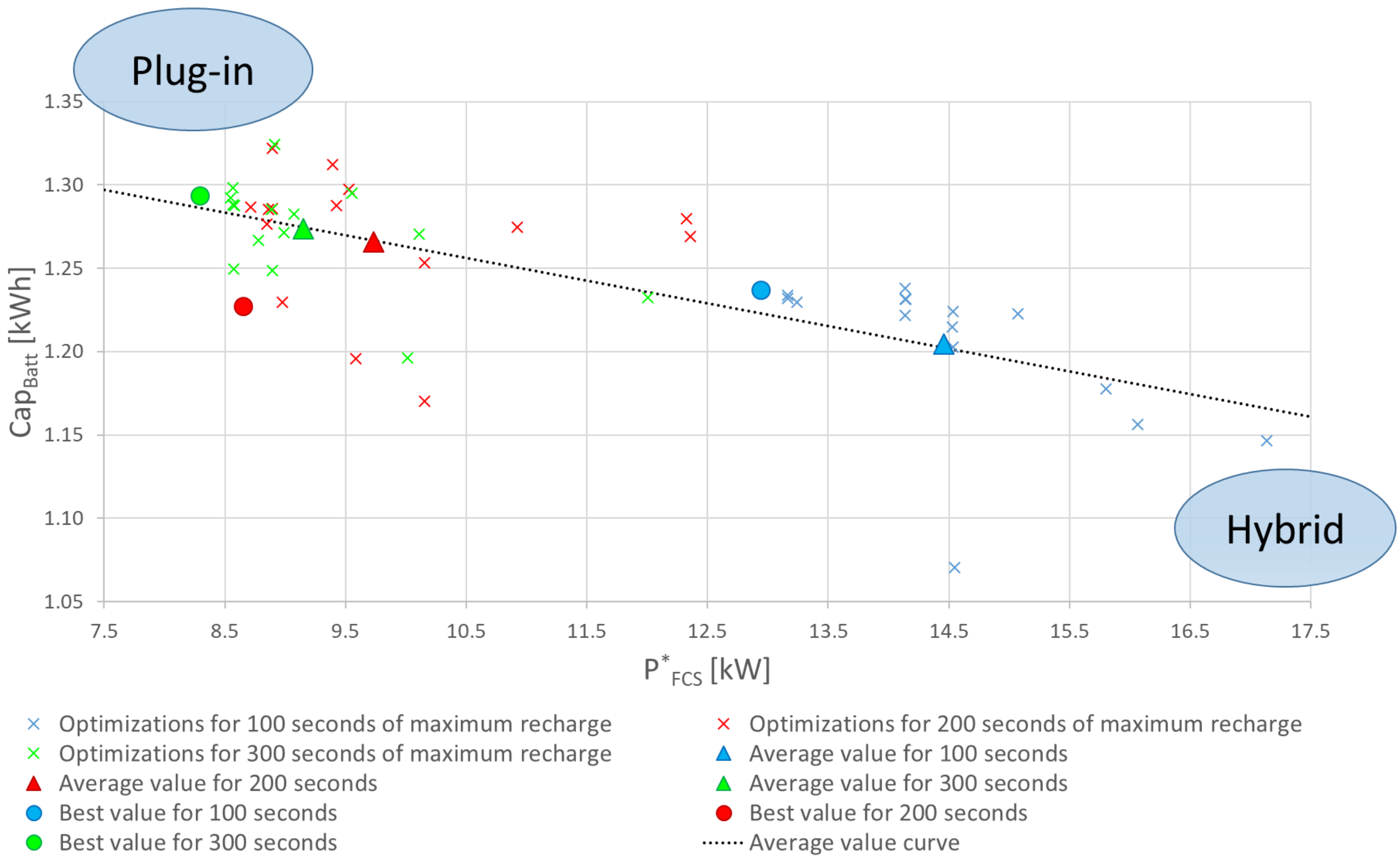

Figure 9: Results related to optimization of the versatile strategy for P^*_{FCref} 20 kW and for the three different limit values set for the battery charging time.

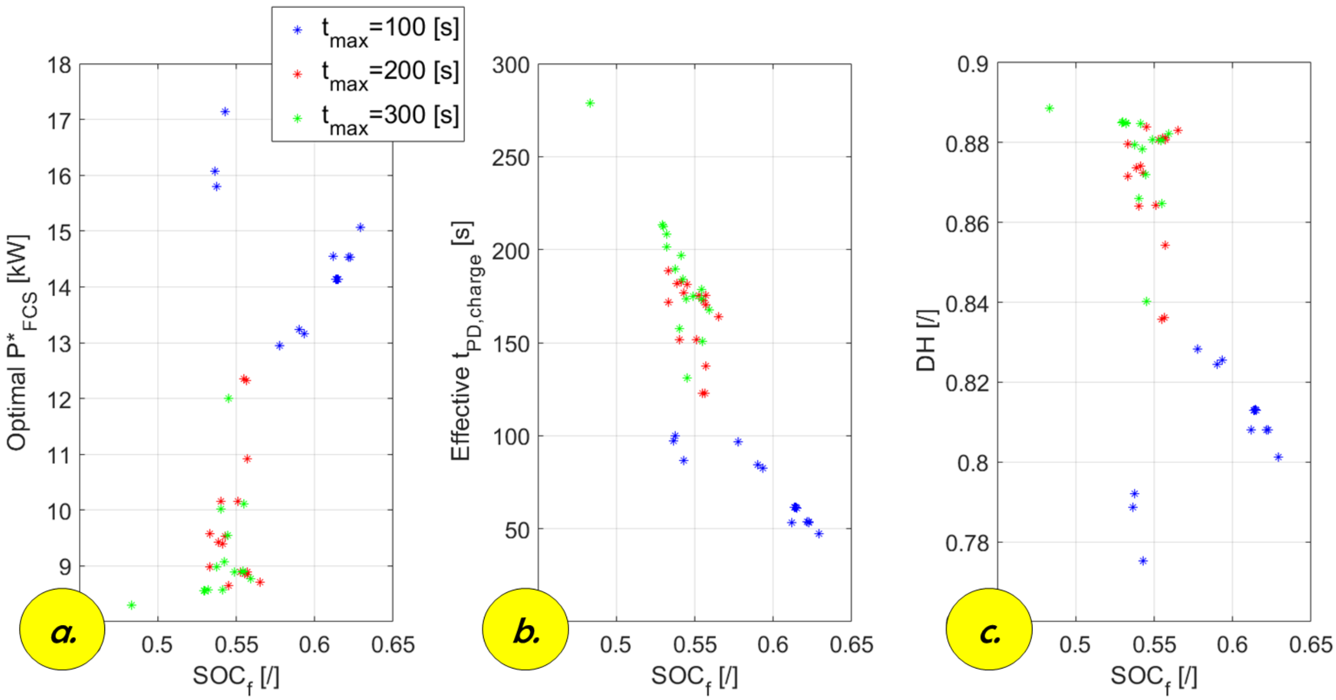

Figure 10: Main control strategies outcomes related to battery final state of charge: a) Optimal fuel cell power [kW], b) Post-driving battery charging time [s], c) Degree of hybridization [/]. Optimization outcomes populating the graphs a-c refer to the optimization task 1 in Table 4

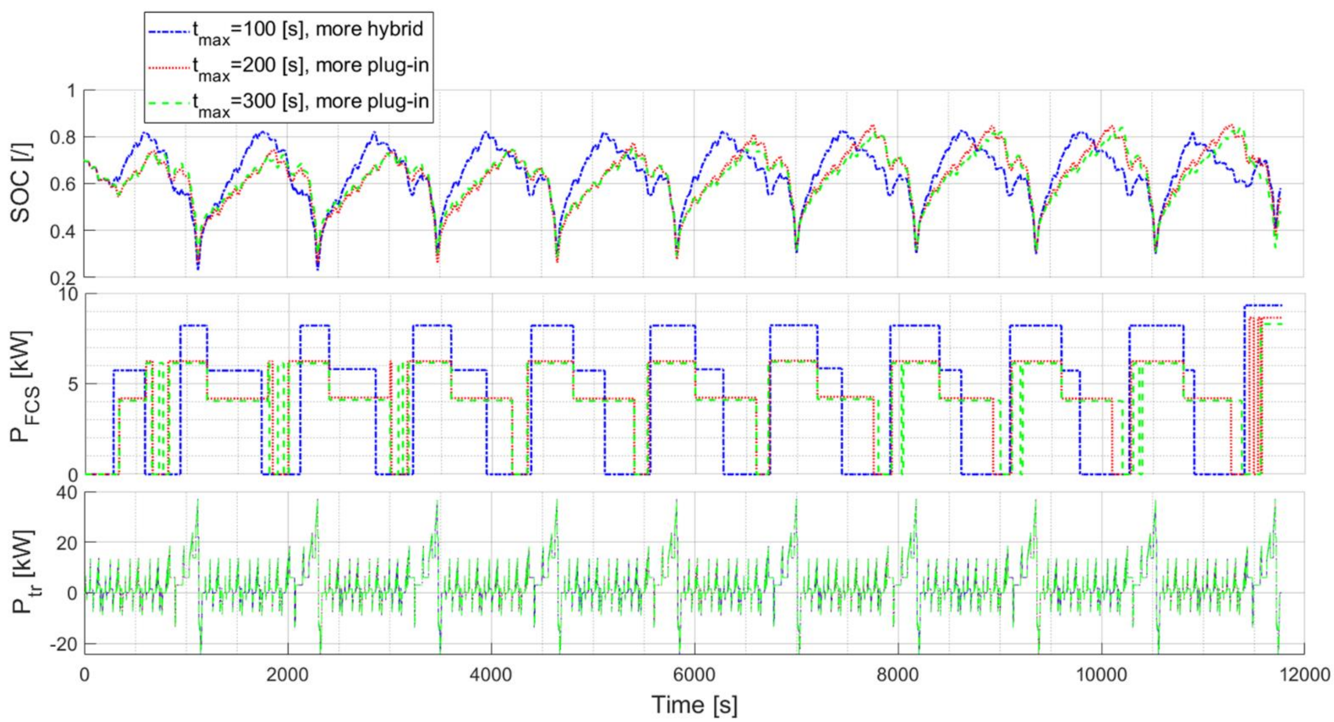

Figure 11: Main time trajectories yielded on output by the simulation of the best case resulting from the optimization task 1 of Table 4: SOC (a), FCS power supply (b), FCHV power demand (c).

5. CONCLUSIONS

A mathematical procedure for the co-optimization of the design and energy management of fuel cell hybrid vehicles was developed and tested on a number of design criteria. Initially, a predefined path travelled by the FCHV was selected and two main variables, that is the FCS power and battery specific energy, were identified. These variables values were obtained by maximizing the hydrogen fuel economy, a performance parameter optimized through a suitable mathematical algorithm, whose development and subsequent assembling activities represent major contributions of current article. Various computational models (i.e. mass model, longitudinal model, battery model, electric motor and FCS models) were used in such a way as to simulate the main FCHV devices behavior. In parallel, a specification independent rule-based control strategy was implemented to determine the vehicle energy management that matches the FCHV design under investigation. Particularly, an intelligent thermostatic control approach (e.g. intermittent operation of the FCS) guided by heuristic rules was initially used. Then, different normalized maps were created. The optimization algorithm used both the component models and the specification independent control strategy, the latter adapted to current powertrain configuration under investigation through suited denormalization of control rules. This way, final outcomes of the optimization consisted not only in determining the optimal values of FCS installed power and battery specific energy, but also in defining the final control policy to be subsequently implemented on-board. Particularly, the procedure was proven effective in accounting for the impact of battery typology (i.e. high-power and high-energy) on fuel economy depending on the working characteristics of selected fuel cell technology (i.e. PEM). Moreover, it was proven suitable to adapt the solution to different control policies, i.e. charge depleting vs. charge sustaining. Particularly, higher post-driving charging time, which was assumed possible to stimulate the procedure in exploring plugin like configurations potentialities, are expected in the CS approach, whereas the CD strategy is characterized by reduced charging periods. Indeed, each scenario offers the possibility of implementing a charge-depleting or charge-sustaining strategy: it is always up to the designer to decide how to realize the interaction between the energy sources in the FCHV. However, the charge-depleting strategy is more useful with powertrain characterized by the highest hybridization level (i.e. plugin), whereas the charge-sustaining is more suitable for a configuration with a lower DH (i.e. hybrid). Hence, when the constraint on the maximum $t_{PD,charge}$ is stricter, the optimization algorithm is oriented towards solutions that are less plugin type. On the contrary, a softer constraint directs the optimization outcomes towards more range-extender (or plugin) configurations, with a consequent preference for a charge-depleting control strategy.

After discussing the procedure and analyzing the obtained solutions, it is worth remarking that it is possible to choose between multiple powertrain configurations that guarantee high performance for the vehicle. Indeed, the optimization algorithm has been conceived considering that the design mostly influences the choice of a solution rather than another. However, this decision could be guided more effectively by resorting to clustering techniques and compaction of the scattered data, in order to direct the designer towards the choice of a single configuration that meets the design constraints and ensures high performance. Additionally, since there is a functional dependence between the masses and the powers of the FCHV components, FE results also influence the other control variables necessary for energy management of the vehicle. In fact, the proposed optimization procedure has allowed to decouple sizing and control problems, thus enhancing a potential comparison with different types of powertrain (e.g. HEVs, FCHVs, BEVs, PHEVs), even in case of different battery or fuel cell technologies. The adoption of the above described algorithm is thus expected to significantly contribute towards the resolution of other problematic issues related to the design of fuel cell hybrid vehicles. For instance, the operating parameters of the control strategy could be modified, (e.g. the times of intervention of the fuel cell during the vehicle travel), in such a way as to follow, as much as possible, the instantaneous power demand at the wheels. Furthermore, an economic analysis could be carried out, thus allowing the possibility of choosing one component rather than another on the basis of technological and production costs, with the same nominal power. Other future tests are aimed to improve results and, above all, obtain solutions that guarantee the highest possible vehicle autonomy.

Vehicle models and control strategy were assembled through a modular approach, thus leaving room for subsequent update and/or upgrade of proposed optimization and control approaches and architectures. Moreover, the cost-function was initially defined aiming at guaranteeing the most efficient functioning of selected battery and fuel cell technologies. Nevertheless future applications can include the addition of further technologies (e.g. both relating to primary propulsion system, e.g. advanced internal combustion engines and solid oxide fuel cells, as well all hybridizing devices, e.g. less expensive batteries, supercapacitors etc.), as well as the analysis of other factors (i.e. components degradation and aging). Therefore, the cost function can be improved and extended in such a way as to extend the validity and applicability of the proposed tool to an extended range of candidate powertrains (hybrid vehicles, solar hybrid cars, pure electric powertrains and so on) and final applications (i.e. not only light duty vehicles, but also buses and heavy duty tracks).

ACKNOWLEDGEMENT

The support provided by University of Salerno is gratefully acknowledged..

NOMENCLATURE

Acronyms

BEV	Battery Electric Vehicle
CD	Charge Depleting
CS	Charge Sustaining
CV	Conventional Vehicle
DH	Degree of Hybridization
EM	Electric Motor
EN	Electric Node
EU	European Union
FC	Fuel Cell
FCEV	Fuel Cell Electric Vehicle
FCHV	Fuel Cell Electric Vehicle
FCS	Fuel Cell System
GB	Gear box
GHG	Greenhouse Gas
H_2	Hydrogen
HEV	Hybrid Electric Vehicle
HT	Hydrogen Tank
ICE	Internal Combustion Engine
LDV	Light Duty Vehicle
Li-ion	Lithium-Ion
NEDC	New European Driving Cycle
OCV	Open Circuit Voltage
OEM	Original Equipment Manufacturer
PD	Post-driving
SOC	State of charge
XEV	Hybrid and Electric Vehicle

Roman symbols

A_v	Vehicle frontal area, (m^2)
Cap	Capacity, (Wh)
C_r	Coefficient of rolling friction, (-)
C_x	Drag coefficient, (-)

E_{charge}	Battery recharge energy, (Wh)
E_{spec}	Specific energy of the battery, (Wh/kg)
F_a	Aerodynamic resistance, (kg·m/s^2)
FE	Fuel Economy, (km/kg)
F_g	Weight force, (N)
F_m	Driving force, (N)
F_r	Rolling resistance, (N)
F_{res}	Resisting force, (N)
g	Gravitational acceleration, (m/s^2)
I	Electric current intensity, (A)
L	Length of vehicle path, (m)
M_{body}	Vehicle body mass, (kg)
M_{CV}	Conventional vehicle mass, (kg)
M_e	Equivalent mass, (kg)
m_{EM}	Electric motor mass, (kg)
m_{FCS}	Fuel cell system mass, (kg)
M_{FCHV}	FCHV mass, (kg)
m_{GB}	Gear box mass, (kg)
M_{HT}	Hydrogen tank mass, (kg)
m_{ICE}	Internal combustion engine mass, (kg)
N_{BC}	Number of battery cells, (-)
P_{aux}	Auxiliaries power, (W)
P_B	Battery pack power, (W)
P_{batt}^*	Battery nominal power, (W)
P_{BC}	Single battery cell power, (W)
P_{BC}^*	Single battery cell nominal power, (W)
P_{EM}	Electric motor power, (W)
P_{EM}^*	Electric motor nominal power, (W)
P_{FCS}	Fuel cell system power, (W)
P_{FCS}^*	Fuel cell system nominal power, (W)
$P_{FCS,charge}$	Fuel cell system recharge power, (W)
P_{ICE}^*	Internal combustion engine nominal power, (W)

P_{stack}	Battery stack power, (W)
P_{tr}	Traction power, (W)
Q_{TOT}	Battery overall capacity, (C)
R_{in}	Internal resistance, (Ω)
t_{drive}	Driving time, (s)
t_h	Time horizon, (s)
t_{max}	Maximum battery recharge time, (s)
$t_{PD,charge}$	Battery charging time, (s)
v	Vehicle speed, (m/s)
V	Voltage, (V)

Greek symbols

ρ_{air}	Air density, (kg/m^3)
ρ_{PtW}	Power to weight ratio, (W/kg)
η_{Batt}	Battery efficiency, (-)
η_{EM}	Electric motor efficiency, (-)
η_{tr}	Traction efficiency, (-)

Subscripts

aux	Auxiliaries
Batt	Battery
BC	Battery Cell
Denorm	Denormalized
f	Final
lo	Lower
Norm	normalized
Ref	reference
Up	upper

REFERENCES

1. Intergovernmental Panel on Climate Change (2015). Climate Change 2014: Mitigation of Climate Change: Working Group III Contribution to the IPCC Fifth Assessment Report. Cambridge: Cambridge University Press.

2. Mi, Z., Guan, D., Liu, Z., Liu, J., Viguié, V., Fromer, N., Wang, Y (2018). Cities: the core of climate change mitigation. *Journal of Cleaner Production*, 207:582-589.

3. Briguglio, N., Andaloro, L., Ferraro, M., Antonucci, V. (2011). Fuel Cell Hybrid Electric Vehicles. *Electric Vehicles - The Benefits and Barriers*, (ed. Seref Soylu), INTECH, Rijeka, pp. 93-118.

4. Weiss, M. A., Haywood, J. B., Schafer, A., Natarajan, V. K. *Comparative Assessment of Fuel Cell Cars*. Technical Report. Massachusetts Institute of Technology, Laboratory for Energy and the Environment, USA. 2003.

5. Onat, N.C., Murat, K.M., Omer, T.O. (2015). Conventional, hybrid, plug-in hybrid or electric vehicles? State-based comparative carbon and energy footprint analysis in the United States. *Applied Energy*, 150:36–49.

6. Katrašnik, T. (2013). Impact of vehicle propulsion electrification on Well-to-Wheel CO_2 emissions of a medium duty truck. *Applied Energy*, 108:236–247.

7. *Inventory of U.S. Greenhouse Gas Emissions and Sinks: 1990-2012*. Technical Report. Environmental Protection Agency. Washington D.C., USA. 2014.

8. Balaguer, J., Ripollés, J. (2018). The dynamics pattern of price dispersion in retail fuel markets. *Energy Economics*, Elsevier, 74(C):546–564.

9. Jacobson, M.Z. Review of solutions to global warming, air pollution, and energy security (2009). *Energy and Environment Science*, 2:148–173.

10. Sorrentino, M., Maiorino, M., Pianese, C. (2013). An integrated mathematical tool aimed at developing highly performing and cost-effective fuel cell hybrid vehicles. *Journal of Power Sources*, vol. 221, pp. 308-317.

11. Shabbir, W., Evangelou, S.A., (2019). Threshold-changing control strategy for series hybrid electric vehicles. *Applied Energy*, 235:761-775.

12. Larminie, J., and Dicks, A., 2002, *Fuel Cell Systems Explained*, Wiley, New York.

13. Tschech, M., Vietor, T., (2015). Cost reduction through cell design optimization for vehicle requirements - From active material to vehicle product portfolio. *World Electric Vehicle Journal*, 7:32-40.

14. Sulaiman, N., Hannan, M.A., Mohamed, A., Ker, P.J., Majlan, E.H., Wan Daud, W.R. (2018). Optimization of energy management system for fuel-cell hybrid electric vehicles: Issues and recommendations. *Applied Energy*, 228:2061-2079.

15. The Fuel Cells and Hydrogen Joint Undertaking (2015). FCH2-JU 2015 calls-ANNEX I Work Plan 2015–Part I Operations, online at http://www.fch.europa.eu/sites/default/files/h2020-wp15-fch_en.pdf.

16. Honda FCX (2015), online at https://en.wikipedia.org/wiki/ Honda_FCX.

17. Toyota Mirai (2015), online at https://en.wikipedia.org/wiki/ Toyota_Mirai.

18. Greene, D.L., Lin, Z. and Dong, J. (2013). Analyzing the sensitivity of hydrogen vehicle sales to consumers' preferences. *International journal of hydrogen energy,* 38:15857-15867.

19. Anandarajah, G., McDowall, W., & Ekins, P. (2013). Decarbonising road transport with hydrogen and electricity: Long term global technology learning scenarios. *International Journal of Hydrogen Energy,* 38:3419-3432.

20. Hung, Y.H., Wu, C.H. (2013). A combined optimal sizing and energy management approach for hybrid in-wheel motors of EVs. *Applied Energy*, 108:236–47.

21. Solano, J., Hissel, D., Pera, M.C., Fail-Safe Power for Hybrid Electric Vehicles: Implementing a Self-Sustained Global Energy Management System (2018). *IEEE Vehicular Technology Magazine*, 13:34-39.

22. Bizon, N. (2018). Real-time optimization strategy for fuel cell hybrid power sources with load-following control of the fuel or air flow. *Energy Conversion and Management*, 157:13-27.

23. Hu, Z., Li, J., Xu, L., Song, Z., Fang, C., Ouyang, M., Dou, G., Kou, G. (2016). Multi-objective energy management optimization and parameter sizing for proton exchange membrane hybrid fuel cell vehicles. *Energy Conversion and Management*, 129:108-121.

24. Zhao, J., Sciarretta, A. (2016). Design and Control Co-Optimization for Hybrid Powertrains: Development of Dedicated Optimal Energy Management Strategy. *IFAC-PapersOnLine*, 49:277-284.

25. Guo, H., Sun, Q., Wang, C., Wang, Q., Lu, S. (2018). A systematic design and optimization method of transmission system and power management for a plug-in hybrid electric vehicle. *Energy*, 148:1006-1017.

26. Sorrentino M., Rizzo G., Arsie I. (2011). Analysis of a rule-based control strategy for on-board energy management of series hybrid vehicles. *Control Engineering Practice*, 19:1433–1441.

27. Samsun, R.C., Krupp, C., Baltzer, S., Gnörich, B., Peters, R., Stolten, D. (2016). A battery-fuel cell hybrid auxiliary power unit for trucks: Analysis of direct and indirect hybrid configurations. *Energy Conversion and Management*, 127:312-323.

28. Sorrentino, M., Mauramati, F., Arsie, I., Cricchio, A., Pianese, C., Nesci, W., "Application of Willans Line Method for Internal Combustion Engines Scalability towards the Design and Optimization of Eco-Innovation Solutions," SAE Technical Paper 2015-24-2397, 2015, https://doi.org/10.4271/2015-24-2397.

29. Agbli, K.S., Hissel, D., Sorrentino, M., Chauvet, F., Pouget, J. (2016). Reverse engineering of a railcar prototype via energetic macroscopic representation approach. *Energy Conversion and Management*, 112:61–80.

30. The Fuel Cells and Hydrogen Joint Undertaking (2014). Multi-Annual Work Plan 2014-2020, online at http://ec.europa.eu/research/participants/data/ref/h2020/other/legal/jtis/fch-multi-workplan_en.pdf.

31. Rousseau, A., Sharer, P., and Ahluwalia, R., "Energy Storage Requirements for Fuel Cell Vehicles," SAE Technical Paper 2004-01-1302, 2004, https://doi.org/10.4271/2004-01-1302.

32. Sciarretta, A., Guzzella, L. (2007). Control of hybrid electric vehicles. *IEEE Control Systems Magazine*, 27:60–70.

33. Zhou, Y., Ravey, A., Péra, M-C. (2019). A survey on driving prediction techniques for predictive energy management of plug-in hybrid electric vehicles. *Journal of Power Sources*, 412:480-495.

34. Sorrentino M., Pianese C., Cilento M. (2016). A specification independent control strategy for simultaneous optimization of fuel cell hybrid vehicle design and energy management. *IFAC-PapersOnLine*, 49:369-376.

35. Arsie, I., Di Domenico, A., Pappalardo, L., Pianese, C., Sorrentino, M. (2006). Steady-state analysis and energetic comparison of air compressors for PEM fuel cell systems. In: *Proceedings of the 4th International Conference on Fuel Cell Science, Engineering and Technology*.19-21 June 2006, Irvine, CA, USA.

36. Song, K., Li, F., Hu, X., He, L., Niu, W., Lu, S., Zhang, T. (2018). Multi-mode energy management strategy for fuel cell electric vehicles based on driving pattern identification using learning vector quantization neural network algorithm. *Journal of Power Sources*, 389:230-239.